THE ASTROPHYSICAL JOURNAL, 546:394–400, 2001 January 1

SINGLE-PULSE CHARACTERISTICS OF THE MILLISECOND RADIO PULSAR PSR B1937+21 AT 430 MHz

F. A. JENET
California Institute of Technology, Space Radiation Laboratory, Pasadena, CA 91125; merlyn@srl.caltech.edu
S. B. ANDERSON
California Institute of Technology, Department of Astronomy, Pasadena, CA 91125; sba@srl.caltech.edu
AND
T. A. PRINCE
California Institute of Technology, Space Radiation Laboratory, Pasadena, CA 91125; prince@srl.caltech.edu
Received 2000 May 19; accepted 2000 August 7

ABSTRACT

The single-pulse characteristics of the millisecond pulsar PSR B1937+21 are studied using the recently installed Caltech baseband recorder at the Arecibo Radio Observatory in Puerto Rico. This is the first such analysis of this object that includes both average intensity pulses as well as "giant pulses." Pulse ensemble-averaging techniques are developed in order to study the characteristics of PSR B1937+21's single pulses since the high time resolution signal-to-noise ratio is less than unity. This analysis reveals that the non–giant pulse radio emission is extremely stable. All observed fluctuations are consistent with diffractive interstellar scattering. Such intrinsic stability has yet to be observed in other radio pulsars.

Subject headings: pulsars: general — pulsars: individual (B1937+21, B0823+26) — radio continuum: stars — stars: neutron

1. INTRODUCTION

In 1982, Backer et al. discovered the 1.56 ms pulsar PSR B1937+21, the fastest pulsar ever observed. Although this pulsar has been known for some time, previous single-pulse studies have been limited to an analysis of "giant pulses" only (Kinkhabwala & Thorsett 2000; Cognard et al. 1996). This is mainly because of its short period, high dispersion measure (DM = 71.0249 pc cm^{-2}), and low observed flux density (240 mJy at 430 MHz). The short period makes it impossible for conventional observing equipment to search for and study micropulse features which are expected to have a timescale of order 1 μs (Hankins 1996). The high dispersion measure necessitates the use of a computationally intensive form of interstellar dispersion removal known as coherent dedispersion (Jenet et al. 1997; Hankins & Rickett 1975). The low observed flux density complicates the study of single pulses because individual pulses are rarely strong enough to be seen above the receiver noise level even at the 305 m radio telescope at Arecibo, PR. Hence, statistical techniques must be employed which average over a large amount of high time resolution data.

Single-pulse studies of PSR B1937+21 and other "millisecond" pulsars are highly desirable for two reasons. First, the origin of the radio emission is, even 32 years after the first pulsar was discovered, still a mystery. The high brightness temperatures ($\sim 10^{25}$ K) associated with the radio emission point to coherent processes which are poorly understood even under less exotic conditions (Melrose 1996). Previous observations of slow pulsars have not constrained the emission mechanism sufficiently; the study of the radio emission properties of millisecond pulsars may provide important new clues. Millisecond pulsars, because of their fast spin periods, have much smaller light cylinder radii, and hence magnetospheres, than slow pulsars. The light cylinder radius (r_{lc}) is defined as $r_{lc} = cP/2\pi$, where P is the pulsar period and c is the speed of light. These objects also have lower surface magnetic field strengths than the general pulsar population (most likely resulting from their having been "recycled" by a binary companion through the accretion of mass and angular momentum). If the radio emission mechanism is at all dependent on such properties, millisecond pulsars should have unique radio properties. The second reason single-pulse studies of millisecond pulsars are important is that millisecond pulsar timing is well known to be an unparalleled source of precision astrometric and astrophysical information. Among factors possibly limiting timing precision is the stability of the average profile, which depends on the properties of single pulses.

Previous single-pulse observations of "slow" pulsars (i.e., pulsars with a period greater than 33 ms) have revealed a wealth of phenomenology (Lange et al. 1998; Hankins 1992, 1996; Stinebring et al. 1984; Hankins & Boriakoff 1978; Ferguson & Seiradakis 1978; Cordes 1975; Rickett 1975). The most common radio emission properties include pulse-to-pulse amplitude fluctuations and pulse shape variations. At least three preferred timescales have been observed: the average profile width, the subpulse width, and the microstructure width (Hankins 1996). These timescales are roughly given by $0.1P$, $0.01P$, and $0.001P$, respectively, where P is the pulse period. Only two pulsars exhibit the phenomenon known as "Giant Pulses": the Crab pulsar (PSR B0531+21) and PSR B1937+21. Giant pulses are extremely powerful radio bursts whose peak flux can reach several thousand times the average pulse flux (Kinkhabwala & Thorsett 2000; Sallmen et al. 1999). For the case of PSR B1937+21, the location of these bursts is restricted to narrow regions of pulse phase. There does not appear to be any preferred location for the bursts emitted by the Crab pulsar.

Single-pulse observations have been limited to approximately 20 "bright" pulsars (Lange et al. 1998; Ferguson & Seiradakis 1978). This sample includes only one millisecond pulsar, PSR J0437−4715 (Jenet et al. 1998). Thus, our current understanding of pulsar radio emission comes from

a small sample of the approximately 1300 known objects (Lyne et al. 2000). Thanks to improvements in computational ability, new techniques can be employed in order to study "weak" pulsars. Weak pulsars are sources whose single-pulse emission cannot be seen above receiver noise levels. These techniques require the calculation of various statistics which are then ensemble averaged over a large number of pulses. These statistics are designed to detect pulse-to-pulse amplitude and shape variations. Millisecond pulsars have the added disadvantage of requiring high time resolution observations in order to properly resolve features within the pulse profile. Standard techniques which average over consecutive time samples in order to increase the single-pulse signal-to-noise ratio do not work well with millisecond pulsars. Ensemble-averaging techniques uncover the single-pulse properties of weak pulsars while maintaining the intrinsic time resolution of the data set, which is 100 ns for the observations described below.

In the next section, the observations are described along with the various preprocessing steps needed to prepare the data for single-pulse analysis. The statistical techniques developed to analyze weak pulsar data are described in § 3. In § 4, the results of this analysis are presented for both PSR B1937+21 and, for comparison, PSR B0823+26. Last, this work is summarized in § 5.

2. OBSERVATIONS AND PREPROCESSING

The data were taken at the 305 m Arecibo radio telescope using the 430 MHz line feed receiver. Both circular polarizations were two-bit complex sampled at a rate of 10 MHz and recorded to tape using the recently installed Caltech baseband recorder (CBR). Further processing of the data was performed at the Caltech Center for Advanced Computation and Research (CACR) using a 256 processor Hewlett-Packard Exemplar.

The two-bit complex samples were unpacked and assigned optimum values in order to minimize signal distortion (Jenet & Anderson 1998). The dual polarization voltage data was adjusted using an empirically derived cross-talk matrix (Stineberg 1982). The effects of the Earth's motion around the Sun was removed by resampling the complex voltage data at a rate necessary to transform the data into the barycentric frame. This rate was calculated using the software package TEMPO (Taylor & Weisberg 1989). The effects of interstellar dispersion were removed by coherently dedispersing the data (Jenet et al. 1997; Hankins & Rickett 1975) at a dispersion measure (DM) of 71.0249 pc cm^{-3}. This value of the DM was measured from the data taken at 430 MHz and agrees with the expected value extrapolated from DM measurements taken by Kaspi, Taylor, & Ryba (1994). For comparison, the slow bright pulsar PSR B0823+26 was also observed and processed as described above using a dispersion measure of 19.463 pc cm^{-3} (Taylor, Manchester, & Lyne 1993).

3. STATISTICAL TECHNIQUES

Previous work on single-pulse emission of bright pulsars has shown that individual pulses tend to have a variety of shapes and sizes (Hankins 1996). The techniques discussed here are designed to identify pulse-to-pulse amplitude and morphological changes in weak pulsar signals. Standard single-pulse analysis techniques attempt to build up the signal-to-noise ratio (S/N) by averaging consecutive measurements of the intensity within a single pulse (Lange et al. 1998; Ferguson & Seiradakis 1978). If the signal-to-noise ratio is larger than ~ 10, then the pulse is used in the analysis. Otherwise, the pulse is not considered. This technique has two major disadvantages: (1) it reduces the time resolution of the data set and (2) it fails to obtain information about weak pulsar signals. Both of these shortcomings preclude the study of fast millisecond pulsars.

In this paper, the signal-to-noise ratio is increased mainly by averaging over pulses rather than consecutive time samples. The information about the single pulses is obtained by calculating ensemble-averaged quantities which are sensitive to pulse-to-pulse fluctuations. This maintains the intrinsic time resolution of the data set, which is 100 ns for the data presented below. The S/N is now determined by the number of pulses in the data set, which is determined by the length of the observation. In principle, one can study the single-pulse properties of any pulsar as long as one observes for "long enough."

3.1. *Ensemble Averaging*

Each of the techniques discussed below makes use of pulse ensemble averaging. This is a standard technique which is normally used to create average intensity profiles and is sometimes referred to as "pulse folding." Since the pulsar period is assumed to be known, a time series representing some relevant quantity, $X(t)$, may be written as $X_i(\phi)$, where ϕ refers to the pulse phase and i represents the pulse number. In the span of one pulsar period, ϕ varies from 0 to 1. Hence, $X_i(\phi)$ represents the quantity X at pulse phase ϕ of the ith pulse in the time series or, equivalently, at time $t = (\phi + i)P$, where P is the pulsar period. The pulse ensemble average of some function of this quantity, $f(X)$, is defined as

$$\langle f(\phi) \rangle = \frac{1}{N} \sum_{i=0}^{N-1} f[X_i(\phi)] \,, \tag{1}$$

where N is the total number of pulses in the data set.

Since the data is discretely sampled in time, the ith pulse is not guaranteed to have a time sample t that corresponds exactly to the desired pulse phase ϕ. Hence, for most cases it is necessary to "bin" the data into a discrete set of N_b pulse phase bins. The ensemble average now becomes

$$\langle f(\phi) \rangle = \frac{1}{N_\phi} \sum_{i=0}^{N-1} \sum_{\delta\phi=-\Delta/2}^{\Delta/2} f[X_i(\phi + \delta\phi)] \,, \tag{2}$$

where N_ϕ is the total number of samples that fell into the phase bin of width $\Delta = 1/N_b$ with a center value of ϕ; N_b may be chosen such that the resulting ensemble average quantity has the same phase resolution as the initial data set.

3.2. *Amplitude Fluctuations*

In order to detect amplitude fluctuations, the pulse ensemble-averaged intensity, $\langle I_s \rangle$, and the intensity squared, $\langle I_s^2 \rangle$, are calculated as a function of pulse phase. For this work, each circular polarization is considered separately. The recorded complex voltage signal, $V(t)$, has both a signal component, $S(t)$, and a system noise component, $N(t)$:

$$V(t) = S(t) + N(t) \,. \tag{3}$$

Using the above relationship and the following definitions for the intensities,

$$I_v(t) = V(t)^* V(t) \,, \tag{4}$$

$$I_s(t) = S(t)^* S(t) \,, \tag{5}$$

$$I_n(t) = N(t)^* N(t) \,, \tag{6}$$

it can be shown that

$$\langle I_v(\phi)\rangle = \langle I_s(\phi)\rangle + \langle I_n(\phi)\rangle \,, \tag{7}$$

$$\langle I_v^2(\phi)\rangle = \langle I_s^2(\phi)\rangle + \langle I_n^2(\phi)\rangle + 4\langle I_s(\phi)\rangle\langle I_n(\phi)\rangle \,, \tag{8}$$

where it is assumed that the signal and the noise are statistically independent and have zero mean values. The signal intensity and the signal intensity squared are obtained by inverting the above equations:

$$\langle I_s(\phi)\rangle = \langle I_v(\phi)\rangle - \langle I_n(\phi)\rangle \,, \tag{9}$$

$$\langle I_s^2(\phi)\rangle = \langle I_v^2(\phi)\rangle - \langle I_n^2(\phi)\rangle - 4[\langle I_v(\phi)\rangle - \langle I_n(\phi)\rangle]\langle I_n(\phi)\rangle \,. \tag{10}$$

Since $\langle I_n(\phi)\rangle$ and $\langle I_n^2(\phi)\rangle$ may be estimated from regions of the data where $I_s(\phi) = 0$ (i.e., the "off pulse" regions), the above expressions can be used to calculate the average intensity and average intensity squared of the pulsar signal alone. For those pulsars where $I_s(\phi)$ never goes to zero, additional observations must be made with the telescope pointing slightly off source in order to measure the noise statistics.

Using $\langle I_s(\phi)\rangle$ and $\langle I_s(\phi)^2\rangle$, the phase-resolved modulation index of the pulsar signal may be calculated from the following definition:

$$m(\phi) \equiv \frac{\sqrt{\langle I_s^2(\phi)\rangle - \langle I_s(\phi)\rangle^2}}{\langle I_s(\phi)\rangle} \,. \tag{11}$$

In general, the modulation index of a statistic X is the square root of the variance, $(\langle X^2\rangle - \langle X\rangle^2)^{1/2}$, divided by the mean value of the statistic, $\langle X\rangle$. If X is a constant, the modulation index is zero. If X varies in any way, the modulation index will be nonzero. Hence, the modulation index is a measure of variation in the statistic. For the relevant case of $X = |Y|^2$, where Y is derived from a complex Gaussian distribution, then $\langle X^2\rangle = 2\langle X\rangle^2$ and the modulation index equals 1. It is instructive to calculate the modulation index of the statistic $Z = AB$, where A and B are uncorrelated random numbers. It turns out that

$$m_Z^2 = m_A^2 m_B^2 + m_A^2 + m_B^2 \,, \tag{12}$$

where m_Z, m_A, and m_B are the modulation indices of the statistics Z, A, and B, respectively. The above equation may be used to show that the modulation index for an amplitude-modulated Gaussian noise process must be strictly greater than unity. Let $A = |Y|^2$, where Y is again derived from a complex Gaussian distribution, and let B be some arbitrary random statistic. Using the fact that $m_A = 1$, equation (12) shows that $m_Z = (1 + 2m_B^2)^{1/2}$, which is always greater than 1.

The phase-resolved intensity modulation index defined above, $m(\phi)$, is a measure of the fluctuations in the pulsar's intensity at a given location in pulse phase. If the statistics of the received electric field are given by a Gaussian distribution, then $m(\phi) = 1$ as discussed above. The presence of any amplitude modulation will cause $m(\phi)$ to be greater than 1. Note that the analysis described above could be performed on Stokes I, but the results would be harder to interpret since the modulation index of Stokes I depends on both the amplitude fluctuations and on correlations between the two polarizations. Hence, analyzing each polarization separately enables a clean determination of the pulse-to-pulse amplitude fluctuations.

3.3. *Pulse Shape Fluctuations and Preferred Timescales*

Although the phase-resolved modulation index is sensitive to pulse shape variations, since such variations cause intensity fluctuations at a single location in pulse phase, this information is not easily extracted from $m(\phi)$. In order to study pulse shape variations, the ensemble-averaged intensity autocorrelation function, $\langle C_{I_s}(\Delta\phi)\rangle$, is calculated and compared with the autocorrelation function of the average intensity $C_{\langle I_s\rangle}(\Delta\phi)$.

Given two measured quantities $X_i(\phi)$ and $Y_i(\phi)$, the cross-correlation function of these quantities computed within a pulse phase region starting at ϕ_0 and ending at ϕ_1 is defined as

$$C_{XY}^i(\Delta\phi) \equiv \frac{1}{\phi_1 - \phi_0} \int_{\phi_0}^{\phi_1} X_i(\phi) Y_i(\phi + \Delta\phi) d\phi \,. \tag{13}$$

If $Y_i = X_i^*$, then the above equation defines the autocorrelation function (ACF) and is denoted as $C_X^i(\Delta\phi)$. For the case of discretely sampled data, the above integral becomes a sum of the discrete points. Note that cyclic boundary conditions are assumed when evaluating the above expression for the case when $\phi + \Delta\phi$ lies outside the interval $[\phi_1, \phi_0]$.

Using the definitions of $V(t)$ and the intensities given in equations (3) and (6), respectively, the ensemble-averaged voltage autocorrelation function,

$$\langle C_V(\Delta\phi)\rangle \equiv \frac{1}{N} \sum_{i=0}^{N-1} C_V^i \,, \tag{14}$$

may be written as

$$\langle C_V(\Delta\phi)\rangle = \langle C_S(\Delta\phi)\rangle + \langle C_N(\Delta\phi)\rangle \,, \tag{15}$$

and the ensemble-averaged intensity autocorrelation function, $\langle C_{I_v}(\Delta\phi)\rangle$, is expressed as

$$\langle C_{I_v}(\Delta\phi)\rangle = \langle C_{I_s}(\Delta\phi)\rangle + \langle C_{I_n}(\Delta\phi)\rangle + 2\langle I_s\rangle\langle I_n\rangle + 2\,\mathrm{Re}\,[\langle C_{S^*S^*}(\Delta\phi)\rangle\langle C_{NN}(\Delta\phi)\rangle] + 2\,\mathrm{Re}\,[\langle C_S(\Delta\phi)\rangle\langle C_N(\Delta\phi)\rangle] \,, \tag{16}$$

where $\langle I_s\rangle$ and $\langle I_n\rangle$ are the average signal intensity and noise intensity, respectively, within the pulse phase window and, consequently, independent of $\Delta\phi$. The above relationships were calculated assuming that the noise and the signal are statistically independent. Using a phase region where $S(\phi) = 0$, all of the noise correlation functions may be estimated and the above relationships may be used to calculate the autocorrelation functions of the signal alone:

$$\langle C_S(\Delta\phi)\rangle = \langle C_V(\Delta\phi)\rangle - \langle C_N(\Delta\phi)\rangle \,, \tag{17}$$

$$\langle C_{I_s}(\Delta\phi)\rangle = \langle C_{I_v}(\Delta\phi)\rangle - C_{I_n}(\Delta\phi) - 2\langle I_s\rangle\langle I_n\rangle - 2\,\mathrm{Re}\,\{[\langle C_{V^*V^*}(\Delta\phi)\rangle - \langle C_{N^*N^*}(\Delta\phi)\rangle]\langle C_{NN}(\Delta\phi)\rangle\} - 2\,\mathrm{Re}\,\{[\langle C_V(\Delta\phi)\rangle - \langle C_N(\Delta\phi)\rangle]\langle C_N(\Delta\phi)\rangle\} \,. \tag{18}$$

The ensemble-averaged intensity autocorrelation function $\langle C_{I_s} \rangle$ is sensitive to the shapes of the individual pulses as well as intensity variations. Fortunately, the effects of intensity variations can be removed by normalizing the autocorrelation function by one of its lags. Hence, $\langle C_{I_s}(\Delta\phi) \rangle / \langle C_{I_s}(\Delta\phi_n) \rangle$ with $\Delta\phi_n$ constant is only sensitive to pulse shape fluctuations. This shape can be compared with the normalized autocorrelation function of the average intensity, $C_{\langle I_s \rangle}(\Delta\phi)/C_{\langle I_s \rangle}(\Delta\phi_n)$. If the curves are identical, then there are no pulse-to-pulse shape variations. Otherwise, $\langle C_{I_s}(\Delta\phi) \rangle / \langle C_{I_s}(\Delta\phi_n) \rangle$ can be used to identify subpulse, micropulse, and other preferred timescales.

One important timescale is the autocorrelation half-width. This is defined as the phase lag, $\Delta\phi_{1/2}$, where the normalized autocorrelation function falls to a value of $\frac{1}{2}$. For $\langle C_{I_s} \rangle$, the half-width refers to the timescale of the individual pulses and, for single-component pulsars, can be directly associated with the subpulse timescale. For $C_{\langle I_s \rangle}$, the half-width refers to the width of the average pulse profile.

4. RESULTS AND DISCUSSION

The average pulse profile $\langle I_s(\phi) \rangle$, the phase-resolved modulation index $m(\phi)$, the average intensity autocorrelation function $\langle C_{I_s}(\Delta\phi) \rangle$, and the autocorrelation function of the average intensity $C_{\langle I_s \rangle}(\phi)$ were calculated in two phase regions of PSR B1937+21 corresponding to the primary and secondary components of this pulsar. For comparison, these statistics were also calculated using data from the bright, slow pulsar PSR B0823+26. Figure 1 shows $\langle I_s(\phi) \rangle$ for both pulsars and thus defines the pulse phase regions used in this analysis. The astrometric and spin parameters for each pulsar are given in Table 1.

4.1. *PSR B0823+26*

PSR B0823+26 is a slow, bright pulsar that has been studied by several investigators (Lange et al. 1998; Rankin & Rathnasree 1995; Wielebinski et al. 1993; Clegg, Fiedler, & Cordes 1993; Romani, Rankin, & Backer 1992). This pulsar demonstrates the most common features of single-pulse phenomenology: extreme amplitude and pulse shape variations. Such behavior has been observed in every pulsar previously studied using standard single-pulse analysis methods (Lange et al. 1998; Hankins 1996; Manchester & Taylor 1977, p. 36). Figures 2*a* and 2*b* show the intensity modulation index and autocorrelation functions, respectively. The phase region used in this analysis is shown in the bottom graph of Figure 1. With $\phi = 0$ defined as the location of the peak in the average intensity profile, ϕ ranges from -80 to 120 milliperiods (mP). This phase region was divided into 1024 phase bins and both $\langle I(\phi) \rangle$ and $\langle I(\phi)^2 \rangle$ were calculated using equations (2), (9), and (10). The resulting time resolution is 104 μs. The intensity autocorrelation function $\langle C_{I_s} \rangle$ was calculated using an I_s that was also binned into 1024 phase bins. Thus, the time resolution of the autocorrelation functions is also 104 μs. Both the

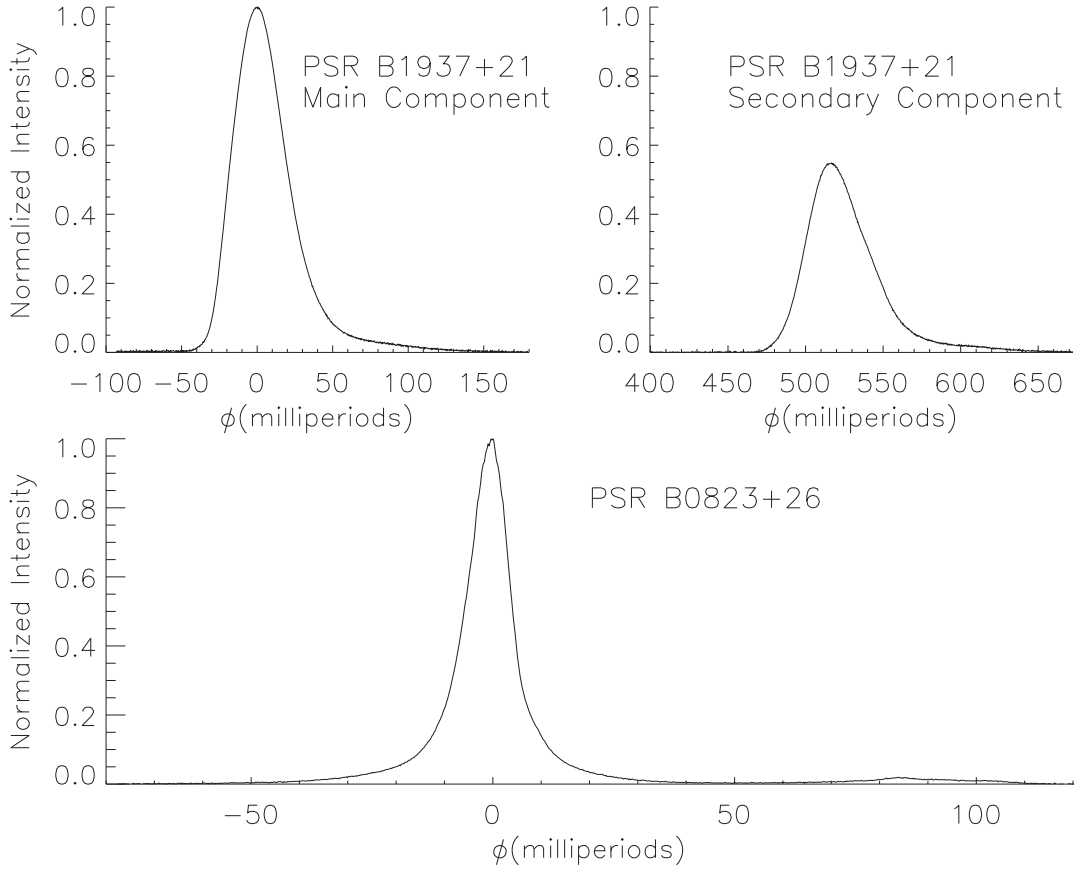

FIG. 1.—Average pulse profiles of pulsars B1937+21 and B0823+26. The profiles have been binned to a time resolution of 0.42 and 104 μs, respectively.

TABLE 1

ASTROMETRIC AND SPIN PARAMETERS FOR PSR B1937+21 AND PSR B0823+26

Parameter	PSR B1937+21	PSR B0823+26
R. A. (J2000)	$19^h39^m38^s.560210(2)$	$8^h26^m51^s.31(2)$
Decl. (J2000)	21°34′08″.14166(6)	26°37′25″.57(7)
Period, P (ms)	1.557806468819794(2)	530.65995906(5)
Period derivative, $\dot{P}$ (10^{-20})	10.51193(2)	1.7236(4)
Epoch of period and position (MJD)	47500.00	42716.5
Dispersion measure (cm^{-3} pc)	71.0249	19.463

NOTE.—For PSR B1937+21 see Kaspi et al. 1994, and for PSR B0823+26 see Taylor et al. 1993.

average autocorrelation function and the autocorrelation function of the average intensity are normalized by the zero lag (i.e., $\Delta\phi = 0$). Approximately 7000 pulses were used in the ensemble average.

As Figure 2 shows, this pulsar exhibits the expected pulse-to-pulse amplitude and shape fluctuations since $m(\phi)$ is significantly greater than 1 and $\langle C_{I_s}\rangle/\langle C_{I_s}(0)\rangle$ differs significantly from $C_{\langle I_s\rangle}/C_{\langle I_s\rangle}(0)$. The ACF half-width of the average profile is approximately 9 mP or 4.8 ms. The half-width of the average ACF is approximately 4.5 mP or 2.4 ms. Thus, the subpulses are, on average, half the width of the average pulse profile. This result is consistent with previous observations.

4.2. *PSR B1937+21*

As shown in Figure 1, this pulsar has two distinct components separated by 516 mP. Approximately 2.9 million pulses were used in the ensemble average. The modulation indices shown in Figures 3*a* and 3*b* were calculated as described in § 3.2 with 1024 phase bins across each region. The resulting time resolution is 0.42 μs. The phase regions for the modulation index spanned from −93 to 180 mP and from 400 to 673 mP for the main component and the secondary component, respectively. For each component, the modulation index reveals two regions: a stable and an unstable region. The unstable region is due to the presence of "giant pulses," a phenomenon that has been previously observed in this pulsar (Kinkhabwala & Thorsett 2000; Cognard et al. 1996). The autocorrelation functions were calculated in a different set of phase regions that did not include the giant pulse region. The ACF phase regions spanned from −119 to 0.13 mP and 401 to 533 mP for the main pulse and the secondary pulse, respectively. The average autocorrelation functions shown in Figures 4*a* and 4*b* were calculated without rebinning the time series, and thus the resulting time resolution is 100 ns. Since $\langle C_{I_s}\rangle$ was calculated using the intrinsic resolution, there is a narrow feature about 100 ns wide starting at lag zero that corresponds to the receiver bandpass. Consequently, the ACFs are normalized by the 300 ns lag or, equivalently, $\Delta\phi = 0.193$ μP. For $C_{\langle I_s\rangle}$, $\langle I_s(\phi)\rangle$ was calculated using 2048 phase bins across each phase window and later interpolated to a time resolution of 100 ns.

For the stable regions in the main pulse and the secondary pulse, $m(\phi) = 1.032 \pm 0.001$ and 1.034 ± 0.003, respectively. These values are consistent with the fluctuations expected from the interstellar medium (Labrecque, Rankin, & Cordes 1994; Cordes et al. 1990). Diffractive interstellar scattering dominates the observed fluctuations since the total observation time ($\approx$4500 s) is significantly less than the refractive scintillation timescale which is approximately 1 yr. Diffractive scintillation causes the pulsar intensity to

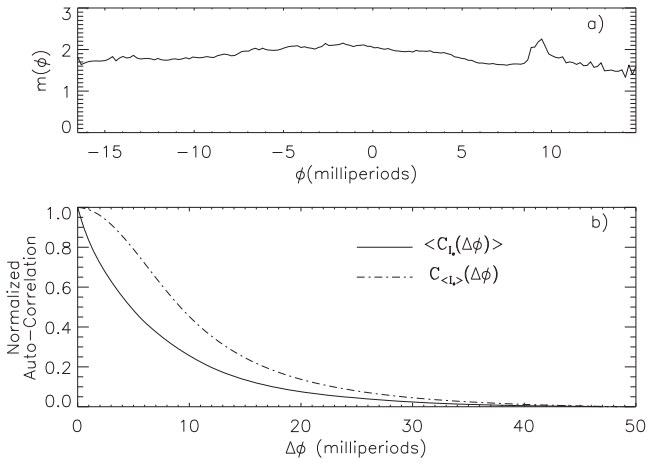

FIG. 2.—Intensity modulation index and the ACFs for PSR B0823+26. The time resolution for both statistics is 104 μs. Only the left circular polarization is displayed. Similar results are obtained with the right circular polarization.

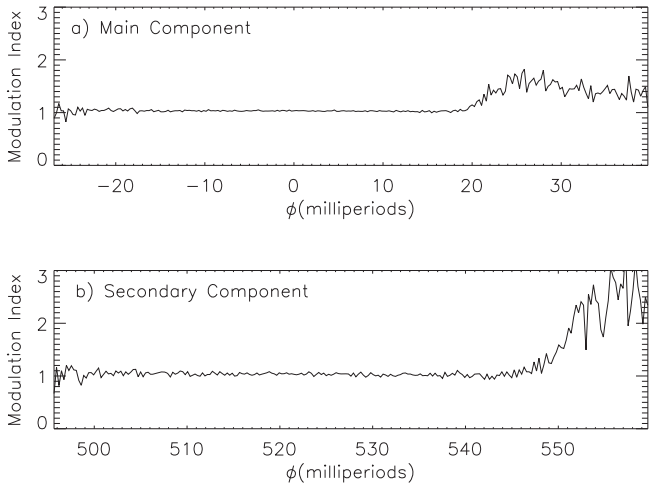

FIG. 3.—Intensity modulation index for both components of PSR B1937+21. The time resolution is 0.42 μs. Only the indices for the left circular polarizations are shown. Similar results are obtained using the right circular polarizations. The above plots are restricted to phase regions where the S/N for the modulation index is large.

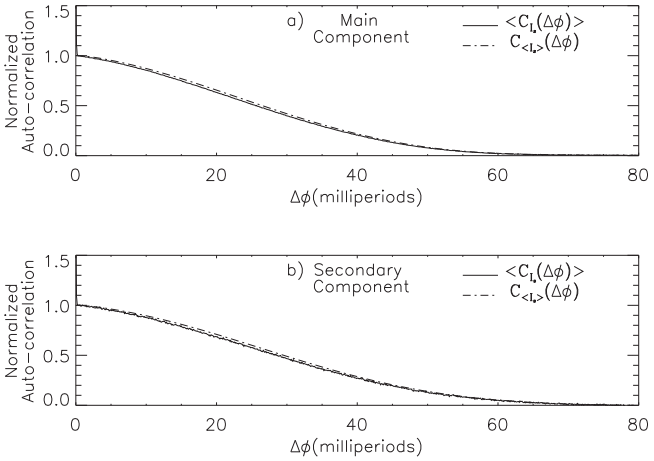

FIG. 4.—Intensity autocorrelation functions for both components of PSR B1937+21 using only left circular polarization. These ACFs were calculated in pulse phase regions that did not include the giant pulses. The time resolution is 0.1 μs. Similar results are obtained using right circular polarization.

fluctuate with a modulation index given by

$$m_{\rm diff} = \frac{1}{\sqrt{N_s}}\,, \tag{19}$$

$$N_s = 1 + \eta\,\frac{\Delta v}{\Delta v_d}\,, \tag{20}$$

where N_s is an estimate of the number of bright features in the spectrum distributed across the observing bandwidth, Δv is the total observing bandwidth, Δv_d is the characteristic bandwidth of the scintillations, and η is an empirically derived packing fraction (Cordes et al. 1990). Using equation (12), the expected modulation index for a complex Gaussian signal modulated by diffractive interstellar scintillation is $m \approx 1.02$–1.04 when $\Delta v_d = 20$ KHz, $\Delta v = 10$ MHz, and $\eta = 0.1$–0.2.

The difference between the ACF half-widths for $\langle C_{I_s}\rangle$ and $C_{\langle I_s\rangle}$ is about 1 μs in both the components. This difference can also be explained by interstellar medium propagation effects. The single-pulse arrival times are expected to vary by an amount given by (Cordes et al. 1990)

$$\delta t = \frac{t_d}{\sqrt{N_s}}\,, \tag{21}$$

$$t_d = (2\pi\,\Delta v_d)^{-1}\,, \tag{22}$$

where t_d is the $1/e$ pulse-broadening time. For the same parameters used to calculate the intensity modulation index, the arrival time fluctuations are given by $\delta t \approx 0.8$–1.1 μs. Hence, the average pulse profile is expected to be slightly wider than each individual pulse creating a difference of approximately 1 μs between the ACF half-widths for $\langle C_{I_s}\rangle$ and $C_{\langle I_s\rangle}$.

These results suggest that the emission in the stable regions of PSR B1937+21 is consistent with amplitude-modulated Gaussian noise where the amplitude function does not vary from pulse to pulse. Such remarkable behavior has never been seen before in any other pulsar.

5. SUMMARY AND CONCLUSIONS

Using pulse ensemble-averaging techniques, we have performed the first single-pulse analysis of PSR B1937+21's non–giant pulse emission. The emission properties appear to differ dramatically from previously studied pulsars. There is no evidence for intrinsic pulse amplitude or pulse shape fluctuations. The small fluctuations detected in the modulation index and the ACFs are consistent with what is expected from propagation effects through the turbulent interstellar medium. Analysis of the millisecond pulsar PSR J0437−4715 (Jenet et al. 1998) revealed that the single-pulse properties of J0437−4715 are similar to the properties of standard slow pulsars. Thus, the unique properties of PSR B1937+21 cannot simply be attributed to this pulsar's fast spin period. Other observations have hinted at PSR B1937+21's remarkable stability. This pulsar's timing noise is extremely small (Kaspi et al. 1994), the linear polarization angle is nearly constant across both profiles (Thorsett & Stinebring 1990), and the giant pulses occur in a restricted region of pulse phase (Kinkhabwala & Thorsett 2000). From a practical standpoint, this object is an ideal polarization calibration source.

Of particular interest is the complete lack of temporal substructure in the stable region. There are no obvious features in the average ACF that would point to subpulses or microstructure. From observations of bright, slow pulsars, the microstructure timescale is expected to be of order 0.5 mP or about 800 ns (Hankins 1996). The fact that $\langle C_{I_s}\rangle$ is smoothly varying with a slope approaching zero and that $\langle C_{I_s}\rangle$ is almost identical to $C_{\langle I_s\rangle}$ is strong evidence for the lack of any substructure down to 200 ns, where the receiver bandpass structure starts to appear. This conclusion is strengthened by the fact that $m(\phi) \approx 1$ over this entire region, suggesting that there are no amplitude fluctuations occurring except those caused by the interstellar medium.

Since a consistent model of pulsar emission has yet to be established, it is difficult to place these observations within a theoretical framework. If the fluctuations observed in other pulsars can be attributed to a small number of emission events, whether coherent or incoherent, then PSR B1937+21's observed stability may be due to an unusually large number of emission events occurring within the on pulse region. Quantifying the number of coherent and/or incoherent events and, consequently, testing the above hypothesis will be the subject of future work. On the other hand, the fluctuations may be due to propagation through a turbulent magnetospheric plasma. In this case, the apparent lack of fluctuations may be attributable to the small light cylinder radius. The relationship between the light cylinder radius and the apparent stability can be probed by applying the ensemble-averaging techniques to a larger sample of millisecond pulsars with a large range of periods. In general, by applying the techniques described in this paper to a large number of weak pulsars, one may uncover correlations between the emission stability and various observable and derivable quantities including period, period derivative, surface magnetic field strength, light cylinder radius, and magnetic inclination angle. Such information will be a valuable tool in understanding the pulsar emission process.

The authors would like to acknowledge Caltech's Center for Advanced Computation and Research for the use of their facilities. We also thank Andrew Melatos for stimulating discussions. This work was supported in part by the National Science Foundation under grant numbers NSF COA 93-18145 and NSF AST 98-19926.

REFERENCES

Clegg, A. W., Fiedler, R. L., & Cordes, J. M. 1993, ApJ, 409, 691
Cognard, I., Shrauner, J. A., Taylor, J. H., & Thorsett, S. E. 1996, ApJ, 457, L81
Cordes, J. M. 1975, ApJ, 195, 193
Cordes, J. M., Wolszczan, A., Dewey, R. J., Blaskiewicz, M., & Stinebring, D. R. 1990, ApJ, 349, 245
Ferguson, D. C., & Seiradakis, J. H. 1978, A&A, 64, 27
Hankins, T. H. 1992, AAS Mtg., 181, 9912
———. 1996, in IAU Colloq. 160, Pulsars: Problems and Progress, ed. S. Johnston, M. A. Walker, & M. Bailes (ASP Conf. Ser. 105; San Francisco: ASP), 197
Hankins, T. H., & Boriakoff, V. 1978, Nature, 276, 45
Hankins, T. H., & Rickett, B. J. 1975, in Methods in Computational Physics: Radio Astronomy, ed. B. Alder, S. Fernbach, & M. Rotenberg (New York: Academic), 55
Jenet, F. A., & Anderson, S. B. 1998, PASP, 110, 1467
Jenet, F. A., Anderson, S. B., Kaspi, V. M., Prince, T. A., & Unwin, S. C. 1998, ApJ, 498, 365
Jenet, F. A., Cook, W. R., Prince, T. A., & Unwin, S. C. 1997, PASP, 109, 707
Kaspi, V. M., Taylor, J. H., & Ryba, M. F. 1994, ApJ, 428, 713
Kinkhabwala, A., & Thorsett, S. E. 2000, ApJ, 535, 365
Labrecque, D. R., Rankin, J. M., & Cordes, J. M. 1994, AJ, 108, 1854
Lange, C., Kramer, M., Wielebinski, R., & Jessner, A. 1998, A&A, 332, 111
Lyne, A. G., et al. 2000, MNRAS, 312, 698
Manchester, R. N., & Taylor, J. H. 1977, Pulsars (San Francisco: W. H. Freeman)
Melrose, D. B. 1996, in IAU Colloq. 160, Pulsars: Problems and Progress, ed. S. Johnston, M. A. Walker, & M. Bailes (ASP Conf. Ser. 105; San Francisco: ASP), 139
Rankin, J. M., & Rathnasree, N. 1995, J. Astrophys. Astron., 16, 327
Rickett, B. J. 1975, ApJ, 197, 185
Romani, R. W., Rankin, J. M., & Backer, D. C. 1992, in IAU Colloq. 128, Magnetospheric Structure and Emission Mechanics of Radio Pulsars, ed. T. H. Hankins, J. M. Rankin, & J. A. Gil (Zielona Góra: Pedagogical Univ. Press), 326
Sallmen, S., Backer, D. C., Hankins, T. H., Moffett, D., & Lundgren, S. 1999, ApJ, 517, 460
Stineberg, D. R. 1982, Ph.D. thesis, Cornell Univ.
Stinebring, D., Cordes, J., Weisberg, J., Rankin, J., & Boriakoff, V. 1984, ApJS, 55, 279
Taylor, J. H., Manchester, R. N., & Lyne, A. G. 1993, ApJS, 88, 529
Taylor, J. H., & Weisberg, J. M. 1989, ApJ, 345, 434
Thorsett, S. E., & Stinebring, D. R. 1990, ApJ, 361, 644
Wielebinski, R., Jessner, A., Kramer, M., & Gil, J. A. 1993, A&A, 272, L13